Three-dimensional numerical simulation of Marangoni flow instabilities in floating zones laterally heated by an equatorial ring

M. Lappa[a)]
MARS (Microgravity Advanced Research and Support Center), Via Gianturco 31-80146, Napoli, Italy and Università degli Studi di Napoli "Federico II," Dipartimento di Scienza e Ingegneria dello Spazio "Luigi G. Napolitano," P.le V. Tecchio 80, 80125 Napoli, Italy

(Received 18 March 2002; accepted 12 December 2002; published 4 February 2003)

Instability of Marangoni convection in floating zones (full zone configuration) of a low Prandtl number fluid under microgravity conditions is investigated by parallel supercalculus and direct three-dimensional and time-dependent simulation of the problem. A parametric analysis (still absent in literature) of the influence of the aspect ratio of the liquid column on the features of the three-dimensional bifurcation of Marangoni flow is carried out. A novel distribution is introduced for the surface heat flux corresponding to the radiative flux generated by a ring heater positioned around the equatorial plane of the full zone at a distance h from the free interface. Axisymmetric computations are used to obtain the steady basic state, then the three-dimensional Navier–Stokes equations are solved to investigate the evolution of azimuthal disturbances. These disturbances always exhibit antisymmetric behavior with respect to the equatorial plane. The mirror symmetry with respect to this plane is broken. Strong interaction occurs in fact between the toroidal convection rolls located in the upper part and lower part of the liquid column. This leads for some values of the aspect ratio to a heretofore unseen ''apparent'' doubling or quadrupling of the azimuthal wave number of the azimuthal velocity distribution in the midplane. The present analysis points out that the instability of the half zone flow is not relevant for the full zone configuration. © *2003 American Institute of Physics.* [DOI: 10.1063/1.1543147]

I. INTRODUCTION

Interest in semiconductor devices has stimulated in the last years the production of high purity single crystals of silicon and other semiconductor materials. Unfortunately, the high chemical reactivity of these substances and their high melting point offer special problems. The most practical solution to these problems has proven to be the floating zone technique, and most of the very pure silicon produced today is processed in this way. Since the floating zone method is capable of growing single crystals with a given orientation, as well as zone refining and leveling, it is ideally suited to the production of silicon crystals for semiconductor devices. By this containerless method, crystals can be grown with less contamination, more homogeneity and higher purity. In these techniques the melt is positioned and solidified without physically contacting the container's wall in order to minimize container-induced contamination and heterogeneous nucleation. The melt zone is produced by heating a short length of feed rod by a heat source such as a ring heater. The rod is slowly moved through the hot zone, and the crystal is obtained by resolidification of the liquid as it is moved away from the heat source.

This method has been often used in the terrestrial environment. However, the floating zone technique is one of the likely candidates of the material processing methods under microgravity conditions. The opportunity of accessing a low gravity environment in the last years has given in fact the possibility of growing larger crystals of higher quality using this method. Buoyancy driven convection which is the most important cause of crystal imperfections is in fact absent in space. However, even in the absence of gravity the presence of free–melt–gas interface at different temperatures induces another undesirable form of convection, the so-called Marangoni convection. The stability of free Marangoni convection in nonisothermal liquid bridges with quasi-cylindrical free surfaces has been the subject of intense research in the last years. These studies are motivated by the fact that flow instabilities in such configurations may be responsible for the appearance of undesirable defects in crystals grown by floating zone technique under microgravity conditions and even under normal gravity conditions. Experiments[1] performed with liquid bridges in the case of transparent liquids (with Prandtl numbers higher than those typical of liquid metals) have shown that for sufficiently small values of the Marangoni number, the convection in the liquid column is laminar, steady and axisymmetrical, but when the Marangoni number exceeds certain critical values depending on the Prandtl number of the liquid, on the aspect ratio (ratio of the length and of the diameter of the liquid zone) and on the boundary conditions, the liquid motion can undergo a transition to an oscillatory three-dimensional complex flow pattern. However, very few works related to the analysis of the Marangoni flow instability in floating zones heated through the interface have appeared in literature and many of these

a)Author to whom correspondence should be addressed. Via Salvator Rosa 53, San Giorgio a Cremano, 80046-Napoli, Italy. Electronic mail: marlappa@marscenter.it, marlappa@unina.it

analyses[2–12] were based on the simplifying assumption of axisymmetric flow. Therefore, due to the experimental evidence of the existence of three-dimensional (3D) states, further investigations on the effect of nonaxisymmetric disturbances are needed. The only available three-dimensional results based on the direct solution of the nonlinear and time-dependent Navier–Stokes equations are due to Baumgartl *et al.*,[13] Croll *et al.*,[14] Levenstam *et al.*[15] and Lan and Chian.[16] They found that for liquid metals the first bifurcation is stationary (i.e., the supercritical state is three-dimensional and steady) and that the regime becomes oscillatory only when the Marangoni number is further increased (second oscillatory bifurcation).

Since these authors were interested mainly to the numerical simulations of their experiments and thus to the critical Marangoni number (Ma_{c2}) for the onset of oscillatory flow (known to be the source of undesirable striations in the crystallized materials), the transition to steady nonaxisymmetric flow (Ma_{c1}) was not determined with any accuracy. Only Lan and Chian[16] determined the first (steady bifurcation) and the second (oscillatory bifurcation) critical Marangoni number. They investigated the case of a floating zone having aspect ratio $A=1.0$ and $\mathrm{Pr}=0.01$. The first critical Marangoni number was also determined by Wanschura *et al.*[17] They carried out a linear stability analysis for the case $\mathrm{Pr}=0.02$ and $A=1.0$.

However, there seems to be a great lack of information dealing with the three-dimensional structure and fundamental properties of the Marangoni flow instability in floating zones heated around the equatorial plane. The available 3D results are fragmentary and incomplete. This is true in particular for the first (steady) bifurcation to 3D flow.

Nevertheless, this instability may play an important role in the float-zone crystallization process. This was proved from an experimental point of view by Camel *et al.*[18] and confirmed by the numerical simulations of Lappa and Savino.[19] ''Weak laminar nonaxisymmetric convection'' in the liquid phase may induce radial segregation with a nonaxisymmetric distribution.[18] Experiments showing these behaviors were carried out during the German Spacelab Mission D-2. Dopant concentration distributions inside the solidified specimen were measured by *a posteriori* spreading resistance techniques. According to the fact that no oscillations were detected in the melt during the flight, on ground analyses of the solidified samples did not show any striation. The concentration distribution, however, was found to be azimuthally distorted from a ''macroscopic'' point of view. The numerical results[19] have confirmed that the steady bifurcation of Marangoni flow can affect the crystallization process.

Aim of the present paper is to perform a parametric analysis (still absent in literature) of the influence of the aspect ratio of the liquid zone on the features of the three-dimensional instability of Marangoni flow under microgravity conditions in the case of a low Prandtl number liquid using direct solution of the nonlinear, three-dimensional, and time-dependent Navier–Stokes equations. Due to the lack of numerical and experimental information, the investigation will be focused in particular on the first (stationary) bifurcation to 3D flow. The present contribution appears as the first attempt to analyze in detail these behaviors.

II. PHYSICAL AND MATHEMATICAL MODEL

A. Modeling the floating zone: "Full zone" configuration

Two models can be used to simulate the flow in a floating zone: ''Half zone'' and ''full zone.''

The half zone configuration is supposed to model the flow in a half of the real floating zone under the constraint that the flow is symmetric by reflection about the plane at midheight between the rods, and that the imposed no-slip condition on this plane does not significantly alter the dynamics. As pointed out by Kasperski *et al.*,[12] the transition of Marangoni flow to a 3D pattern in the case of the half zone flow may be not relevant for the real floating zone since, there, the mirror symmetry with respect to the equatorial plane could be broken. For this reason, even if the half zone has become over the years a very important ''paradigm'' model for fundamental research, the assumption of the full zone model is the only way to ''capture'' in detail the mechanisms of the instability of Marangoni flow occurring in real floating zones.

The ends of the domain are plane and isothermal as in the case of the half zone model, but the supporting disks are posed at the same temperature. The presence of a ring heater around the equatorial plane of the zone is simulated imposing a specified heat flux distribution on the free surface with a maximum of the flux in correspondence of the equatorial plane (in the half zone model the end disks are held at the maximum and minimum temperatures, respectively, whereas in the full zone model the temperature maximum occurs between the disks). Note that the full zone model has a disadvantage due to the fact that the temperature difference driving the surface flow between the ends of the domain and the equatorial cross section cannot be fixed *a priori* since it is a consequence of the flow itself (i.e., ΔT is established by the convective and heat transport through the liquid zone).

B. Basic assumptions

The geometry of the problem is shown in Fig. 1(a). The floating zone is confined between two coaxial cylindrical disks of diameter D placed $2L$ apart, heated at the midheight by an external ring heater. The upper and lower solid–melt interfaces are assumed to be flat and they are kept at the melting point temperature T_m. The maximum temperature on the free surface (this temperature corresponds to the equatorial plane if $\mathrm{Ma}<\mathrm{Ma}_{c1}$) is denoted by $T_{\max}$. The temperature difference acting on the free surface is a result of the Marangoni flow itself and follows from the calculations. The temperature difference achieved for the 2D solution used as initial condition for the 3D computations is denoted by $\overline{\Delta T}(\overline{T}_{\max}-\overline{T}_m)$ and is used for the definition of the Marangoni number. The overbar denotes dimensional quantities. The liquid is assumed homogeneous and Newtonian, with constant density and constant coefficients; viscous dissipa-

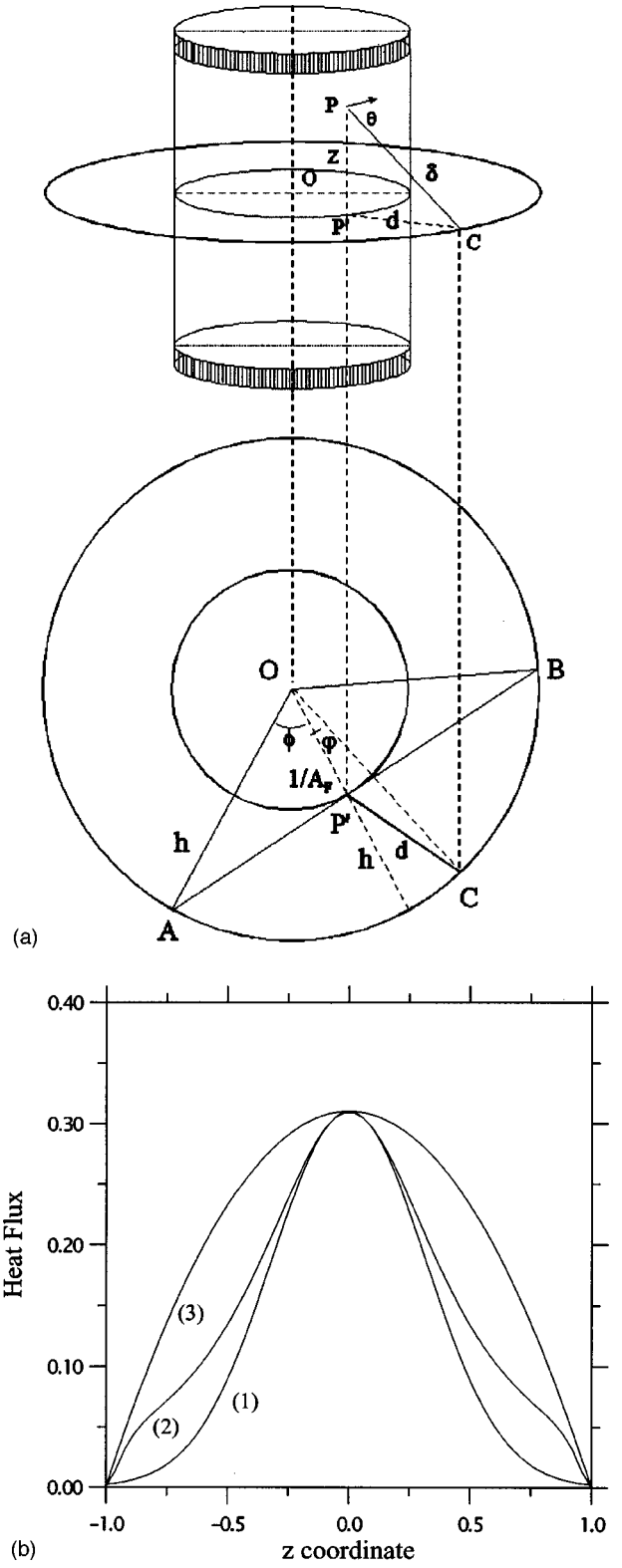

FIG. 1. Sketch of the floating zone and its boundary conditions: (a) Full zone configuration, (b) heat flux profile $J(z)$: (1) $J \propto \exp(-cz^2)$, (2) flux generated by the ring heater for $A_F=1.0$ and $\Phi=\epsilon \overline{Q}=1$ [w], (3) $J \propto (1-z^2)$.

tion is negligible. The liquid filling the bridge is bounded by an axisymmetric liquid–gas interface with a surface tension $\overline{\sigma}$ exhibiting a linear decreasing dependence on the temperature

$$\overline{\sigma}=\overline{\sigma}_o-\overline{\sigma}_T(\overline{T}-\overline{T}_m), \tag{1}$$

where $\overline{\sigma}_o$ is the surface tension for $\overline{T}=\overline{T}_m$ and $\overline{\sigma}_T=-d\overline{\sigma}/d\overline{T}>0$.

The interface is assumed to be nondeformable and axisymmetric around the z axis. The geometrical aspect ratio of the full zone A_F is defined as $A_F=2L/D$; the aspect ratio of the corresponding half zone (half of the considered full zone) is defined as $A_H=L/D=A_F/2$.

C. Nondimensional field equations and boundary conditions

The flow is governed by the continuity, Navier–Stokes and energy equations, that in nondimensional conservative form read

$$\underline{\nabla}\cdot\underline{V}=0, \tag{2a}$$

$$\frac{\partial \underline{V}}{\partial t}=-\underline{\nabla}p-\underline{\nabla}\cdot[\underline{V}\underline{V}]+\mathrm{Pr}\,\underline{\nabla}^2\underline{V}, \tag{2b}$$

$$\frac{\partial T}{\partial t}=-\underline{\nabla}\cdot[\underline{V}T]+\nabla^2 T, \tag{2c}$$

where V and p are the nondimensional velocity and pressure, Pr is the Prandtl number ($\mathrm{Pr}=\upsilon/\alpha$, υ is the kinematic viscosity and α is the thermal diffusivity). The nondimensional form results from scaling the cylindrical co-ordinates $(\overline{r,z})$ by half of the axial distance between the circular disks (L) and the velocity components $(\overline{V}_z,\overline{V}_r,\overline{V}_\varphi)$ by the energy diffusion velocity $V_\alpha=\alpha/L$; the scales for time and pressure are, respectively, L^2/α and $\rho\alpha^2/L^2$. The temperature is measured with respect the initial temperature $\overline{T}_m$.

$$T=(\overline{T}-\overline{T}_m). \tag{3}$$

The boundary conditions on the rigid disks are the no-slip condition and the temperature conditions:

$$\underline{V}(z=-1,r,\varphi,t)=0;\quad T(z=-1,r,\varphi,t)=0,$$

$$0\leqslant r\leqslant 1/A_F;\quad 0\leqslant\varphi\leqslant 2\pi, \tag{4a}$$

$$\underline{V}(z=1,r,\varphi,t)=0;\quad T(z=1,r,\varphi,t)=0,$$

$$0\leqslant r\leqslant 1/A_F;\quad 0\leqslant\varphi\leqslant 2\pi. \tag{4b}$$

The boundary conditions on the free surface ($r=1/A_F$, $-1\leqslant z\leqslant 1$, $0\leqslant\varphi\leqslant 2\pi$) are the kinematic conditions of a stream surface (zero normal velocity), the Marangoni conditions (shear stress balance) and the condition of prescribed heat flux.

$$V_r(z,r=1/A_F,\varphi,t)=0, \tag{5a}$$

$$\frac{\partial V_Z}{\partial r}(z,r=1/A_F,\varphi,t)=-\mathrm{Ma}_r\frac{\partial T}{\partial z}(z,r=1/A_F,\varphi,t), \tag{5b}$$

$$r\frac{\partial V_\varphi}{\partial r}(z,r=1/A_F,\varphi,t)-V_\varphi(z,r=1/A_F,\varphi,t)$$

$$=-\mathrm{Ma}_r\frac{\partial T}{\partial \varphi}(z,r=1/A_F,\varphi,t), \tag{5c}$$

where $\mathrm{Ma}_r=\sigma_T L/\mu\alpha$ and the reference Marangoni number Ma is defined as $\mathrm{Ma}=\mathrm{Ma}_r(\overline{\Delta T})$.

$$\frac{\partial T}{\partial r}(z,r=1/A_F,\varphi,t)=J(z). \tag{5d}$$

Many models have been proposed in literature to simulate surface heating due to a ring heater [i.e., to define $J(z)$].

In general the methods used by the different investigators to model the heating source (ring heater, circular arrangement of halogen lamps, ellipsoid–paraboloid mirror furnace, laser with axisymmetric ring shape, etc.) fall into two categories: Specifying the ambient temperature distribution or finding the power requirement for producing a desired $\overline{\Delta T}$ on the free surface. For the first case the ambient temperature distribution is assumed to be known. According to Chen and Chu,[7] Chen and Wu,[8] however, in real systems the ambient temperature distribution is unknown *a priori* whereas the power supplied by the external source is a known parameter. This led some investigators to model the surface heating, assuming a certain law of variation (i.e., parabolic, exponential) and fixing the total input requirement $(\overline{\Delta Q})$.

In the present paper a new distribution is introduced for the heat flux, corresponding to the radiative flux generated by a ring heater having negligible thickness and positioned around the equatorial plane of the full zone at a distance h from the free surface.

Each point C disposed on the ring heater between the points A and B, see Fig. 1(a), gives a radiative contribution to the generic point P of the free surface; this contribution is

$$j(z)=\left(\frac{1}{L\lambda\overline{\Delta T}}\right)\frac{1}{4\pi}\frac{\epsilon\overline{Q}}{\delta^2}\cos(\vartheta), \tag{6}$$

where $\overline{Q}$ is the power supplied to the ring heater, δ the distance between the points C (on the ring heater) and P (on the free surface) and θ is the angle between $\underline{n}$ (unit vector orthogonal to the free surface in P) and the direction PC.

Thus the total flux in P can be computed as

$$J(z)=\frac{1}{4\pi}\left(\frac{\epsilon\overline{Q}}{L\lambda\overline{\Delta T}}\right)\int_{-\tilde{\phi}}^{\tilde{\phi}}\frac{\cos(\vartheta)}{\delta^2}d\varphi, \tag{7}$$

where

$$\delta^2=\frac{1}{A_F^2}[(1+hA_F)^2+1-2(1+hA_F)\cos\varphi+z^2], \tag{8a}$$

$$\cos(\vartheta)=\frac{(1+hA_F)\cos\varphi-1}{\sqrt{[(1+hA_F)^2+1-2(1+hA_F)\cos\varphi+z^2]}}, \tag{8b}$$

$$\tilde{\phi}=a\cos\frac{1}{(1+hA_F)}, \tag{8c}$$

$h=0.5$ and the value of the emissivity ϵ of the free surface is given in Ref. 20.

The heat transport is, therefore, maximum in the surface region and tries to change the driving temperature gradients in the surface by itself (i.e., via the Marangoni stress acting on the free interface). Figure 1(b) shows the surface heat flux profile computed according to (7) and other analytical laws plotted for the same value of the maximum heat flux at the equatorial plane.

III. NUMERICAL METHOD

A. Solution method

Equations (2a)–(2c) were solved numerically in primitive variables by a time-explicit finite-difference method

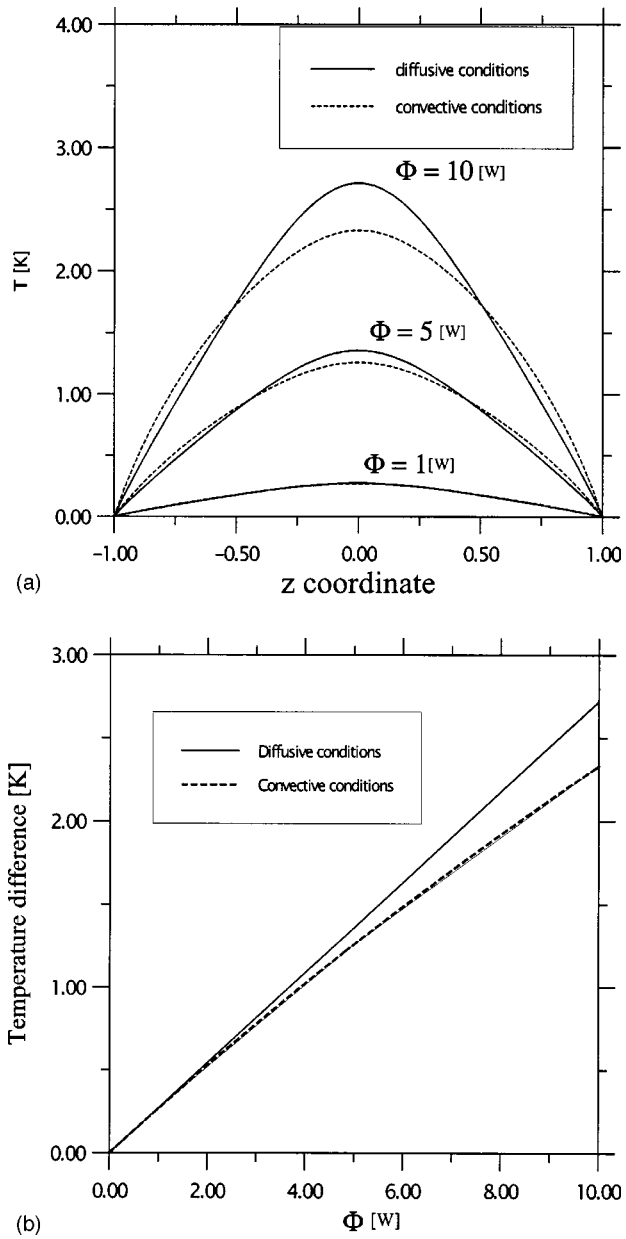

FIG. 2. (a) Temperature distribution on the free surface (Pr=0.01, $A_F=1.0$, $\Phi=\epsilon\overline{Q}$), (b) temperature difference vs $\Phi=\epsilon\overline{Q}$.

TABLE I. (a) Grid refinement study for the accuracy of the basic state solution ($A_F=1.0$, Ma=10). (b) Influence of the number of points in azimuthal direction ($A_F=1.0$).

(a)

Grid	$\Psi_{\max}$	$V_{z\,\max}$	$V_{r\,\max}$
25×15	0.100 36	1.431	0.5674
30×18	0.099 55	1.392	0.5707
35×21	0.099 15	1.365	0.5734
40×25	0.099 04	1.346	0.6004
45×27	0.099 01	1.342	0.6157
50×30	0.099 00	1.337	0.6223
55×33	0.099 00	1.331	0.6227

(b)

$N_z\times N_r\times N_\phi$	Ma_{c1}
53×31×23	12.873
53×31×35	12.442
53×31×42	12.415
53×31×47	12.413

TABLE II. Critical azimuthal wave number, critical Marangoni number, interaction factor and mesh vs the aspect ratio.

A_F	L [cm]	m	Ma_{c1}	N	$N_z\times N_r\times N_\phi$
0.2	0.1	9	22.157	2	29×100×100
0.3	0.15	6	15.340	2	33× 70× 89
0.4	0.2	4	12.280	2	35× 57× 79
0.5	0.25	4	9.760	2	41× 45× 75
0.6	0.3	3	13.597	2	43× 38× 63
0.7	0.35	2	10.90	2	45× 35× 49
0.8	0.4	2	12.028	2	49× 31× 47
0.9	0.45	2	11.326	2	51× 31× 47
1.0	0.5	2	12.413	2	53× 31× 47
1.1	0.55	2	14.910	2	57× 30× 39
1.2	0.6	2	15.086	2	63× 30× 37
1.3	0.65	1	11.350	4	69× 30× 35
1.5	0.75	1	10.154	4	79× 29× 35
1.8	0.9	1	10.364	4	95× 29× 33
2.0	1.0	1	9.923	4	100× 29× 33

(SMAC method). The domain was discretized with a uniform cylindrical mesh and the flow field variables defined over a staggered grid. Forward differences in time and central-differencing schemes in space (second-order accurate) were used to discretize the energy and momentum partial differential equations. Parallel supercalculus was used due to the enormous time required for the computations. The problem is split in two problems, one parabolic and the other elliptic. A parallel algorithm, explicit in time, is utilized to solve the parabolic equations. A parallel multisplitting kernel is introduced for the solution of the pseudo-pressure elliptic equation, representing the most time-consuming part of the algorithm. A grid-partition strategy is used in the parallel implementations of both the parabolic equations and the multisplitting elliptic kernel. A message passing interface (MPI) is coded for interprocessor communications. For further details on the numerical method see, e.g., Lappa and Savino.[21]

In the analyses of Chenier *et al.*,[9] Chen and Roux,[10] and Kasperski *et al.*,[12] the stability boundaries were computed directly as function of the input power supplied to the heating source (i.e., their Marangoni number is based directly on ΔQ). In the present paper the Marangoni number is based on the temperature difference ($T_{\max}-T_m$) obtained for the 2D solution (basic state) used as initial condition for the 3D computations. This definition is more close to experimental criteria and allows to compare with previous critical Marangoni numbers obtained in the case of ''half zone'' model. It has been pointed out in the previous paragraphs, however, that in the case of a full zone model the temperature gradient acting on the free surface is not known ''*a priori*.'' Its value in fact is affected by the strength of the Marangoni convection. Due to Marangoni convection, the surface temperature profile departs from the corresponding diffusive one (i.e., obtained in the case Ma=0). This is clearly shown in Fig. 2. The ΔT acting on the free surface is smaller than that obtained for Ma=0. For this reason, for the present simulations, the Marangoni number has not been fixed *a priori*, but has been computed as function of the power supplied to the heating device.

The critical Marangoni number Ma_c is defined as a threshold value at which the growth rate of the disturbances is zero. In the present study, in order to determine the growth rate constant, the power supplied to the system is changed at several times in a stepwise manner. The results of the different runs give the growth rate constant as a function of the Marangoni number. The growth rate is computed analyzing the behavior of the time-dependent history of the maximum of the azimuthal velocity (posed in logarithmic scale versus time) on the free surface (the same criterion has been used by other investigators see, e.g., Leypoldt *et al.*[23]). According to linear stability criteria (see, e.g., Chen and Roux[10]), the critical Marangoni number then is determined as the Marangoni number at which the growth rate becomes zero.

B. Validation of the numerical procedure

To check that the code is able to ''capture'' the physical instabilities of Marangoni flow, the first critical Marangoni number in the case $A_F=1.0$ and Pr=0.01 has been computed and compared with the results of Lan and Chian.[16] For this case they predict $\mathrm{Ma}_{c1}\cong 12$. The critical Marangoni number determined by the present numerical computations is $\mathrm{Ma}_{c1}=12.413$ (3% greater than their value) with $m=2$. This comparison provides a sufficient validation of the present numerical code.

TABLE III. Physical properties of silicon melt.

Melting point temperatute Tm [K]	1685
Density ρ [gr/cm^3]	2.42
Thermal diffusivity α [cm^2/s]	$2.44\,10^{-1}$
Kinematic viscosity ν [cm^2/s]	$2.45\,10^{-3}$
Prandtl number	0.01
Thermal conductivity λ [W/cmK]	0.64
Surface tension σ [dyne/cm]	$7.33\,10^{2}$
σ_T [dyne/cmK]	$1\,10^{-1}$
Emissivity [-]	0.3

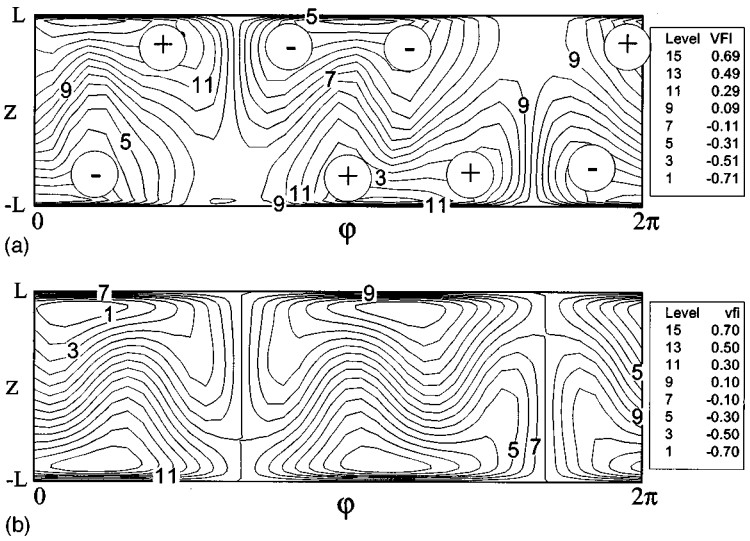

FIG. 3. (a) Surface azimuthal velocity distribution at the 3D stationary state ($A_F=1.3$, $m=1$, Ma≅30, $\Phi=2.54$ [w], numerical results); (b) plot of the analytical expansion of the surface azimuthal velocity: $[\tilde{F}_1(z)\sin(m\varphi+G_o)-\tilde{F}_2(z)\sin(Nm\varphi+NG_o)]$, $\tilde{F}_1(z)=z(1-z^{20})^2$, $\tilde{F}_2(z)=0.3(1-z^2)^2$, $m=1$, $N=4$, $Go=1$.

C. Grid refinement study

Table I(a) shows the grid refinement study carried out for the 2D basic state.

This study has been conducted also on the influence of the number of points used in azimuthal direction $N\varphi$ [Table I(b)]. For different values of the aspect ratio, the number of points collocated in the axial direction and in the radial direction has been changed according to the length and to the radius of the liquid column, respectively (see Table II). The criterion for the number of points to be collocated in azimuthal direction has been based on the value of the azimuthal wave number m. Preliminary computations with a coarse number of points in azimuthal direction have been performed in order to determine m, then $N\varphi$ has been selected according to the formula $N\varphi/m\cong 30$ for $m=1$, $N\varphi/m\cong 24$ for $m=2$, $N\varphi/m\cong 20$ for $m=3$ and $m=4$ $N\varphi/m\cong 15$ for $m=6$, $N\varphi=91$ for $m=9$.

IV. RESULTS

Because of the considerable computation time involved (each run on a DS20 Compaq parallel computer required about twelve days of CPU time) the investigation has been restricted to only one value of the Prandtl number (Pr=0.01 corresponding to silicon melt; see Table III for the properties of liquid silicon) but different aspect ratios have been investigated (see Table II). Figures 3–14 show the structure of the flow field in different planes and sections for different values of the aspect ratio at the 3D stationary state. Note that no *a priori* known small azimuthal disturbances have been superimposed on the solution to facilitate the transition. Disturbances are freely produced in a spontaneous way by the computations.

A. Effect of the aspect ratio and description of the spatial organization

Table II shows that the azimuthal wave number of the critical mode (m) is a function of the aspect ratio of the full zone. In particular the critical number is $m=1$ for $1.3\leqslant A_F\leqslant 2.0$, whereas higher values have been found for lower aspect ratios: $m=2$ for $0.7\leqslant A_F\leqslant 1.2$, $m=3$ for $A_F=0.6$, $m=4$ for $0.4\leqslant A_F\leqslant 0.5$, $m=6$ for $A_F=0.3$ and $m=9$ for $A_F=0.2$ (very short liquid column). These results suggest an empirical correlation between the geometrical aspect ratio and the critical azimuthal wave number of the instability similar to that found by previous analyses in the case of the half zone configuration. This correlation is

$$mA_F\cong 2. \tag{9}$$

The flow structure is related to the value of m and hence depends on the value of the aspect ratio. The higher is m, more complex is the flow organization. When A_F is decreased and m increases, multicellular structures are formed.

Figures 5, 9, and 12 show for different values of the aspect ratio the axial velocity in cross-sections orthogonal to the liquid column axis. Figures 6, 10, and 13 show the azimuthal velocity in the same sections. In azimuthal direction there are $2m$ convective cells. Moreover, the isocontour lines of the axial velocity in the generic section z describe in this plane well defined curves whose shape is related to the value of the azimuthal wave number.

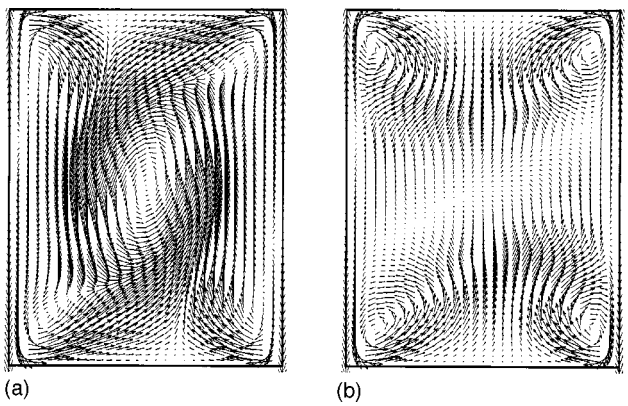

FIG. 4. Velocity field in the meridian plane ($A_F=1.3$, Ma≅30, $\Phi=2.54$ [w], $m=1$); (a) $\varphi\cong 3\pi/4$, (b) $\varphi\cong 5\pi/4$.

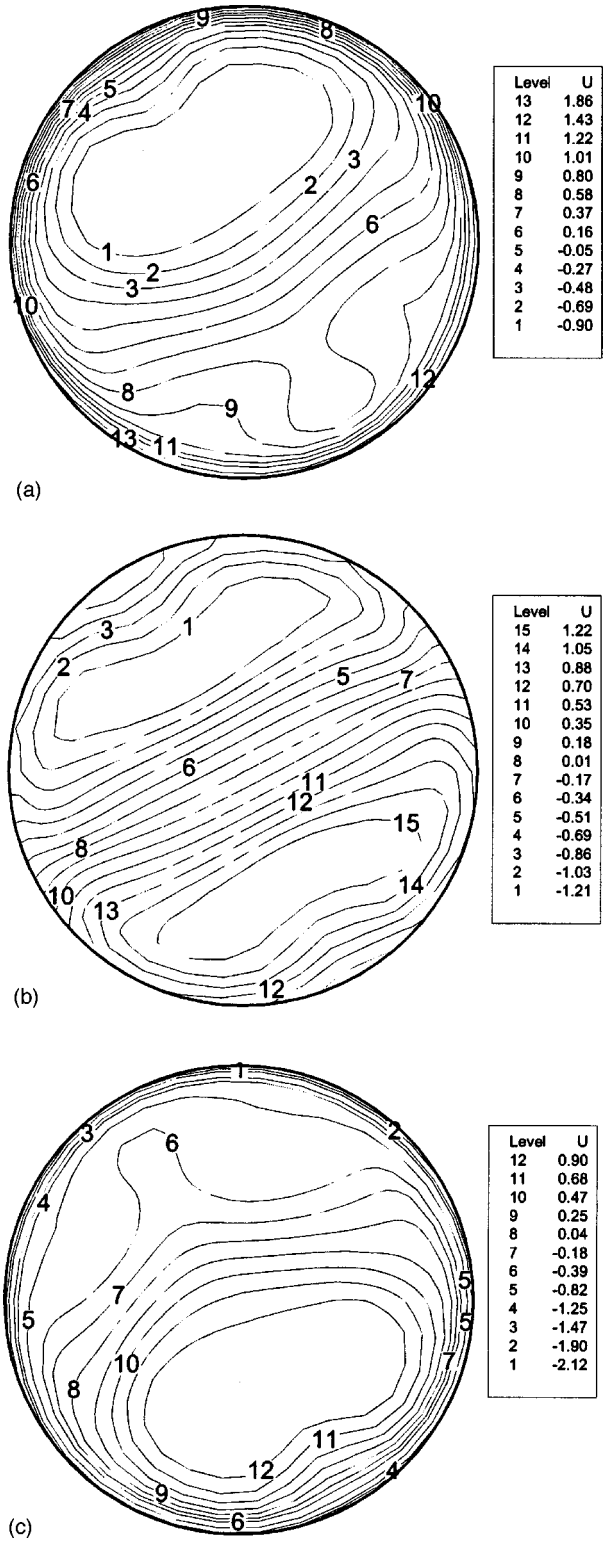

FIG. 5. Structure of 3D Marangoni flow with $m=1$, $A_F=1.3$, Ma≅30, $\Phi=2.54$ [w]: (a), (b), (c) axial velocity in the cross-sections $z=0.5$, $z=0$, $z=-0.5$.

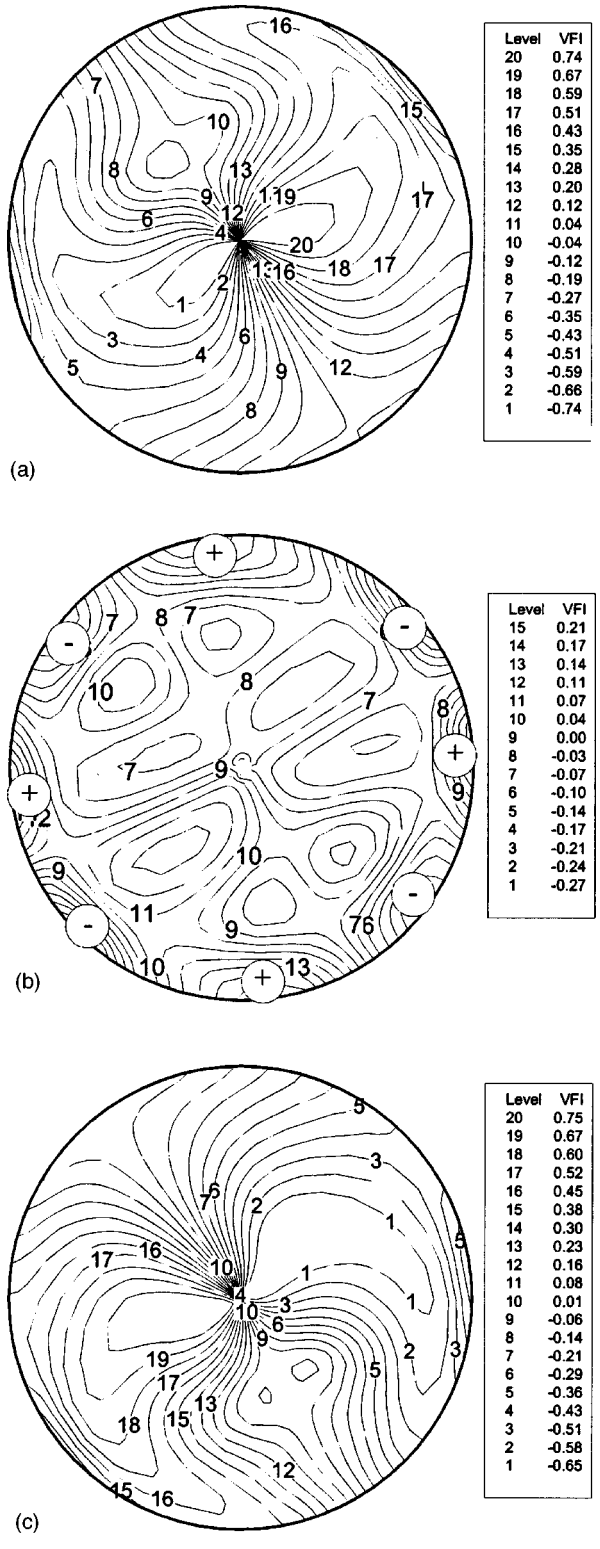

FIG. 6. Structure of 3D Marangoni flow with $m=1$, $A_F=1.3$, Ma≅30, $\Phi=2.54$ [w]: (a), (b), (c) azimuthal velocity in the cross-sections $z=0.5$, $z=0$, $z=-0.5$.

For a more detailed description of the space organization of the thermofluid-dynamic field it is necessary to distinguish even critical wave numbers from odd ones.

Wave numbers $m=1$, $m=3$, and $m=9$ belong to the class of ''asymmetrical'' modes; $m=2$, $m=4$, and $m=6$ are instead ''symmetric'' modes. More generally, when the critical disturbance number (m) is odd, the flow is asymmetrical in each meridian plane of the liquid bridge.

For even critical wave numbers, the flow field structure is on the whole three-dimensional and depends on the azimuthal co-ordinate, but in each axial plane the velocity and the temperature fields are symmetric with respect to the axis.

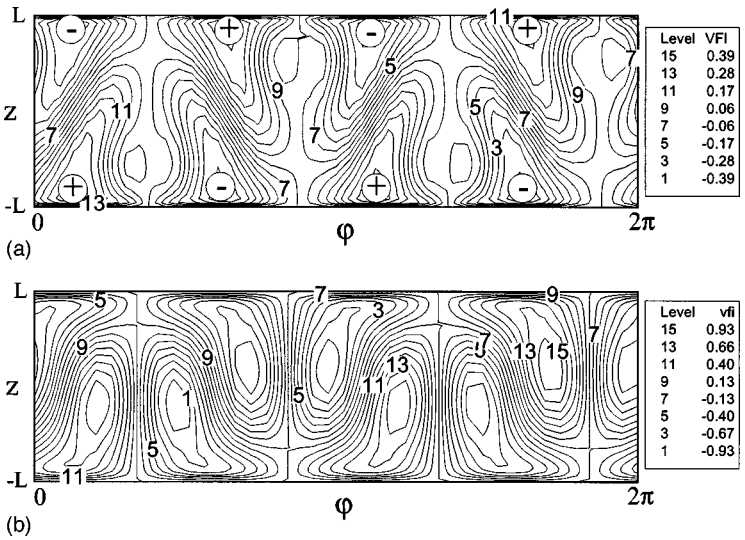

FIG. 7. (a) Surface azimuthal velocity distribution ($A_F=0.8$, $m=2$, Ma≅30, $\Phi=4.57$ [w], numerical results); (b) plot of the analytical expansion of the surface azimuthal velocity: $[\tilde{F}_1(z)\sin(m\varphi+G_o)-\tilde{F}_2(z)\sin(Nm\varphi+NG_o)]$, $\tilde{F}_1(z)=z(1-z^{20})^2$, $\tilde{F}_2(z)=(1-z^2)^2$, $m=2$, $N=2$, $Go=1$.

For $A_F=1.3\,(m=1)$ the flow is no longer separated in cells being positioned in the lower and upper part of the meridian plane. The left vortex cell in the lower part and the right vortex cell in the upper part merge giving rise to a vortex extended along the whole axial plane of the full zone; the other cells contract up to be confined in the left and right corners of the upper and lower half, respectively [Fig. 4(a)]. The behavior is similar for $A_F=0.6\,(m=3)$; in this case (not shown) however since the liquid zone is short and since Marangoni convection, being a surface phenomenon, is confined to regions near the free surface, coalescence of opposite convection cells (leading to a single vortex pervasive throughout the meridian plane) does not occur. For $A_F=0.8\,(m=2)$ and $A_F=0.3\,(m=6)$ the flow is symmetric with respect to the axis but asymmetric with respect to the equatorial plane. Figures 8(a) and 8(b) $(m=2)$ show that the vortex cells in the lower (or upper) half puff up protruding in the upper (lower) half of the floating zone. For both even and odd critical wave numbers the mirror symmetry with respect to the midplane is broken.

Table II shows that, while the critical wave number changes with the aspect ratio, the critical Marangoni number does not change much and tends to increase with decreasing the aspect ratio (see, e.g., Fig. 15 where the growth rates as function of the Marangoni number and the determination of the first critical Marangoni number are shown for different values of the aspect ratio).

B. Comparison with the half zone

The half zone has proven to be over the years a very important model for fundamental research. For instance, by half-zone-based analyses investigators elucidated that the three-dimensional Marangoni flows are initiated through different mechanisms, i.e., inertia instability of the axial shear layer below the free surface for small Pr fluids and hydrothermal wave for large Pr fluid case. It however cannot be used to obtain quantitative data about the floating zone technique. The Ma_{c1} values computed for the half zone model by several investigators[22–28] in fact are two times higher than the values calculated for the present case of full zone model (see Fig. 16). The reason for this difference is, that the independence and separation of the flows in the upper and the lower half of a full zone, which is stated by using a half zone model, is not true. The instability of the half zone flow is not relevant for the full zone configuration since, as pointed out by the present analysis, the mirror symmetry with respect to the equatorial plane is broken. The Ma_c value for a half zone is likely to be higher than that for a full zone because of the additional no-slip condition at the heated disk and the reduced degrees of freedom compared to the full-zone configuration.

Note that, contrary to the conclusions of the present paper, Wanschura *et al.*[17] found that the scenario of development of the instability for small Prandtl numbers in full zone is similar to that for half zone model. This difference can be explained according to the different boundary conditions introduced by the two analyses. Wanschura *et al.*[17] used a fixed temperature profile whereas in the present investigation a more realistic condition has been adopted: A fixed surface heat flux (the surface temperature profile is not fixed *a priori*, but determined as part of the computations and as function of the power supplied to the heating device). Generally the surface temperature profile in the 3D state is neither axisymmetric nor mirror symmetric with respect to the equatorial plane. If the surface temperature distribution is fixed, full liquid zones behave (approximately) as half zones since interaction between the upper and lower parts is somehow prevented.

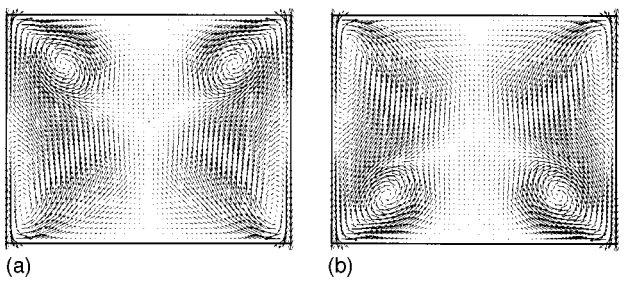

FIG. 8. Velocity field in the meridian plane ($A_F=0.8$, Ma≅30, $\Phi=4.57$ [w], $m=2$); (a) $\varphi\cong\pi/2$, (b) $\varphi\cong\pi$.

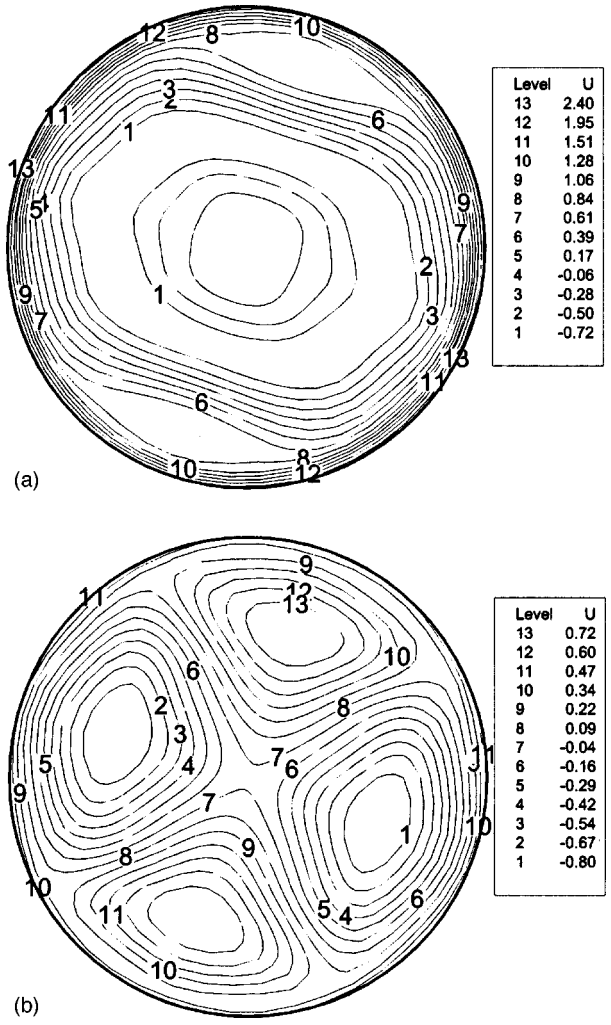

FIG. 9. Structure of 3D Marangoni flow with $m=2$, $A_F=0.8$, Ma≅30, $\Phi=4.57$ [w]: (a), (b) axial velocity in the cross-sections $z=0.5$, $z=0$.

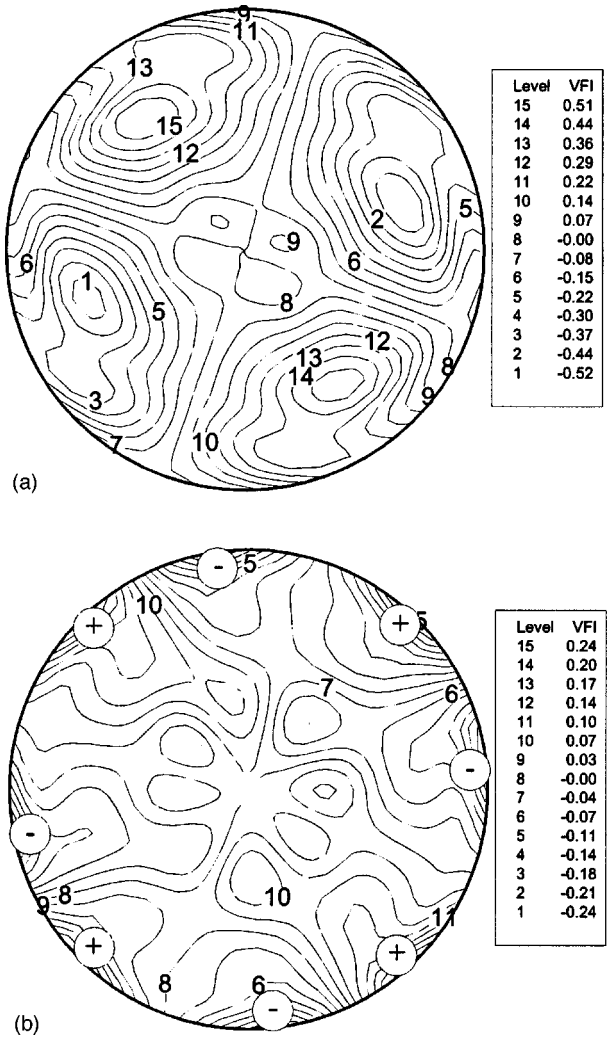

FIG. 10. Structure of 3D Marangoni flow with $m=2$, $A_F=0.8$, Ma≅30, $\Phi=4.57$ [w]: (a), (b) azimuthal velocity in the cross-sections $z=0.5$, $z=0$.

Fixing the temperature profile leads in fact to a surface temperature that is mirror symmetric with respect to the equatorial plane regardless of the flow conditions. Since the surface Marangoni flow is forced [Eqs. (5b) and (5c)] to "follow" the steepness of the imposed temperature profile, this may artificially force the system to maintain symmetric behavior preventing transition to three-dimensional state and mutual interaction of the toroidal convection rolls. This of course leads to larger values of the critical Marangoni number (due to the reduced degrees of freedom). If the surface temperature is constraint-free the behavior is different.

With regard the azimuthal structure of the flow field, note that in the case of half zone configuration it is known that discrete wave numbers of disturbances are selected out of the full spectrum of disturbances because the convection roll is closed in a special zone geometry. Since the instability is hydrodynamic in nature (as pointed out by Levenstam *et al.*[24]), i.e., it does not depend on the behavior of the temperature field (for this instability the temperature field simply acts as a driving force for the velocity field), the selection rule is given simply by the constraint that the azimuthal wavelength must be an aliquot of the toroidal vortex core circumference and by the fact that the convection roll is limited axially by the presence of the sidewalls. According to this theory the critical wave number is related to the axial

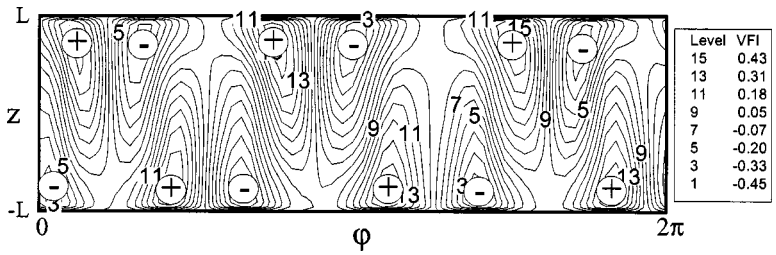

FIG. 11. Surface azimuthal velocity distribution at the 3D stationary state ($A_F=0.6$, $m=3$, Ma≅30, $\Phi=6.27$ [w]).

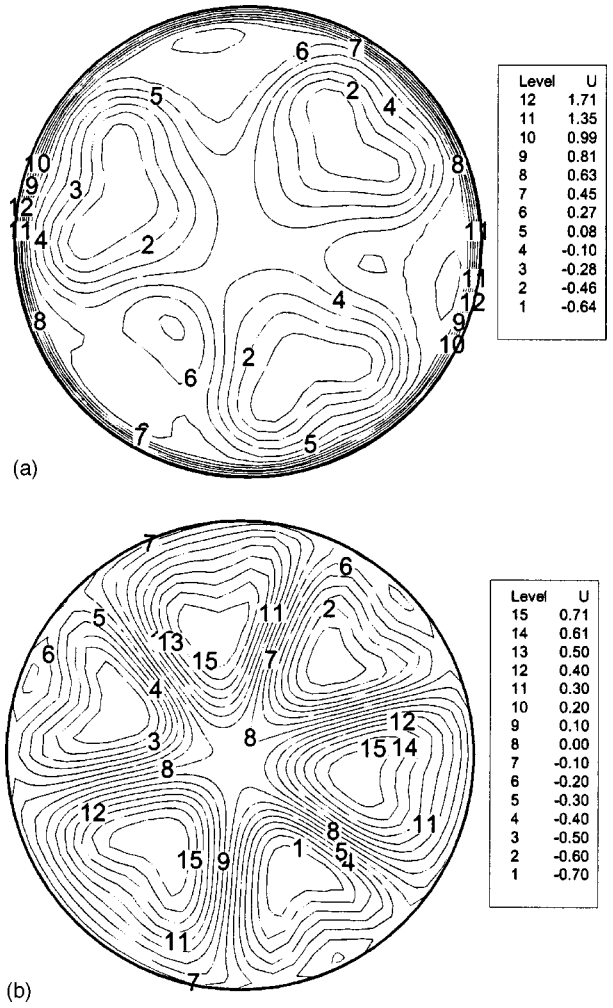

FIG. 12. Structure of 3D Marangoni flow with $m=3$, $A_F=0.6$, Ma≅30, $\Phi=6.27$ [w]: (a), (b), axial velocity in the cross-sections $z=0.5$, $z=0$.

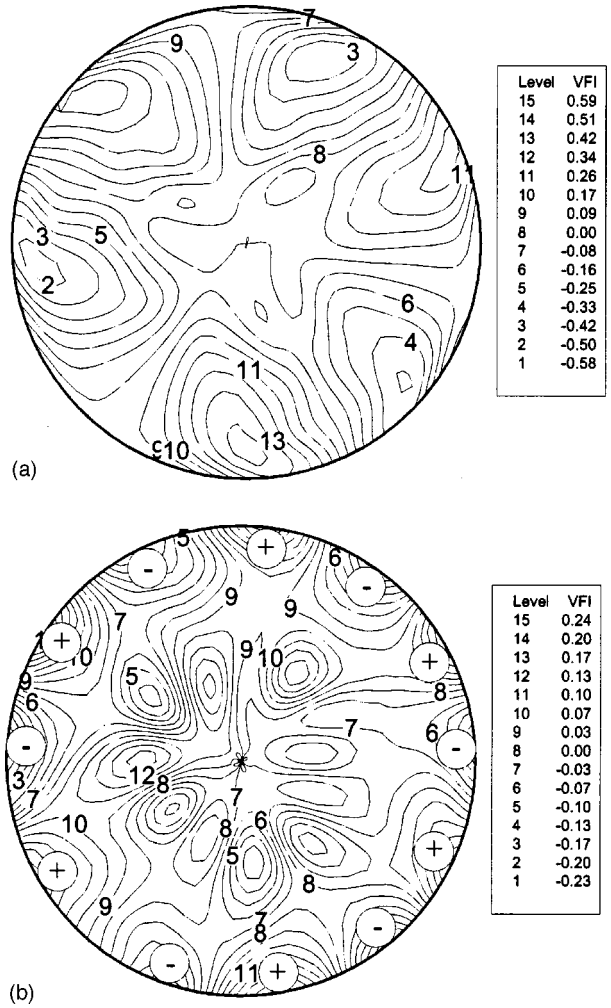

FIG. 13. Structure of 3D Marangoni flow with $m=3$, $A_F=0.6$, Ma≅30, $\Phi=6.27$ [w]: (a), (b) azimuthal velocity in the cross-sections $z=0.5$, $z=0$.

length of the half zone and to its diameter D, i.e., it scales with the parameter $A=L/D$:

$$mA_H \cong 1, \tag{10}$$

the same behavior holds in the case of full zone model. For this configuration, however, the convection roll is bounded by a wall from one side and it is free to interact in nonlinear way with the opposite convection roll from the other side (see the next paragraph). This leads to lower values of the critical Marangoni number and to different structure of the azimuthal flow for some value of the aspect ratio (for $A_H=0.25$, $A_H=0.35$, and $0.65 \leqslant A_H \leqslant 0.85$ the half and full zone configurations are characterized by different values of the azimuthal wave number; see Fig. 17).

C. The symmetry of the disturbances

After the bifurcation, the flow field can be interpreted as the superposition of steady sinusoidal azimuthal disturbances to the axisymmetric state. For each of the two toroidal convection rolls in the upper and lower part of the floating zone, this superposition can be expressed as

$$\begin{aligned} F_i(r,z,\varphi,t) &= F_o(r,z) + f_i(r,z,\varphi,t) \\ &= F_o(r,z) + \tilde{f}_i(r,z,t)\sin(m_i\varphi + G_i), \\ i &= \text{up} \quad (0<z<1), \quad \text{low} \quad (-1<z<0), \end{aligned} \tag{11}$$

where $F_i(r,z,\varphi,t)$ is the generic flow field variable, the subscript (o) refers to the axisymmetric state, m_i is the azimuthal

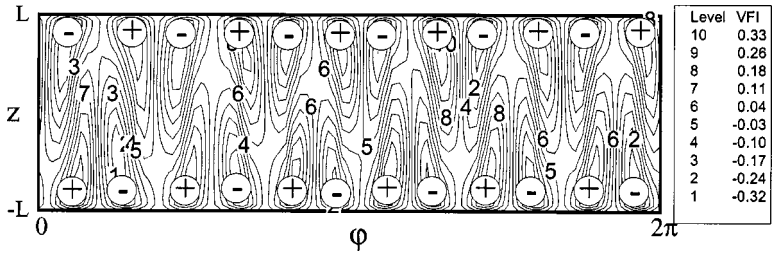

FIG. 14. Surface azimuthal velocity distribution at the 3D stationary state ($A_F=0.3$, $m=6$, Ma≅30, $\Phi=12.3$ [w]).

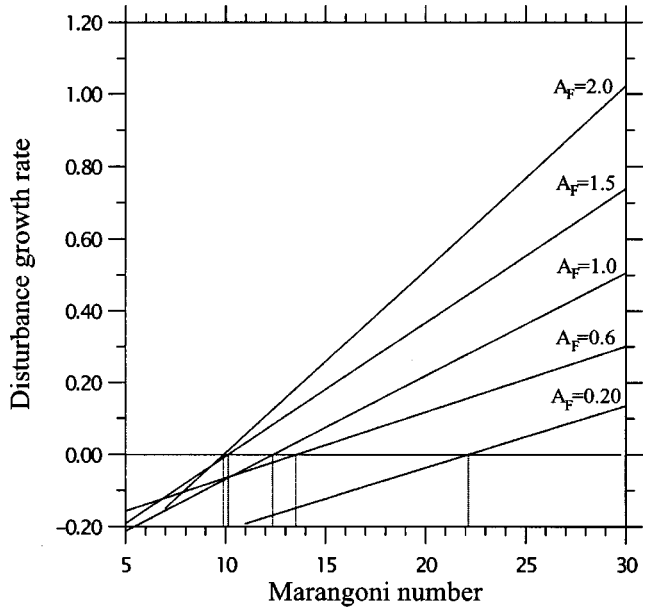

FIG. 15. Growth rates as function of the Marangoni number and determination of the first critical Marangoni number for different values of the aspect ratio.

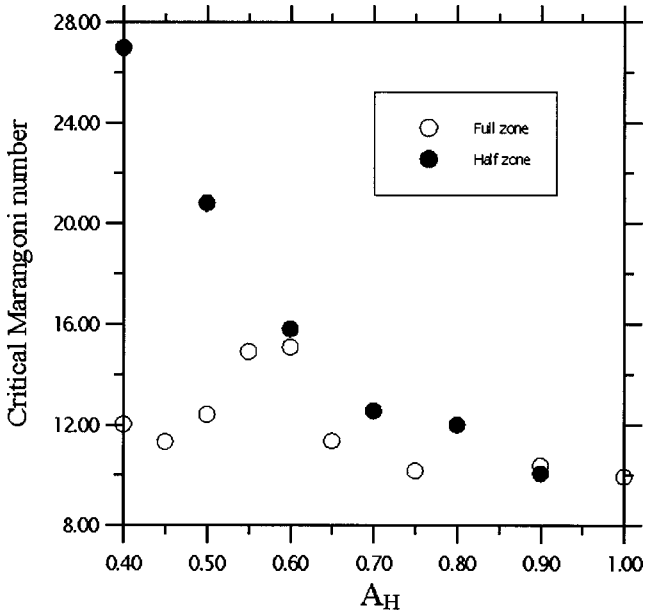

FIG. 16. Comparison between the critical Marangoni number of the full-zone configuration (present results) and available results [Imaishi *et al.* (Refs. 25 and 26) and Chen *et al.* (Ref. 28)] dealing with the half zone configuration (Pr=0.01).

wave number that represents the number of spatial periods in the azimuthal direction, G_i is a constant phase shift related to the azimuthal position of the disturbance extrema for the considered convection roll (i=low, convection roll in the lower part of the full zone; i=up, convection roll in the upper part of the full zone). The present numerical results show that $m_{\mathrm{up}}=m_{\mathrm{low}}$ and $\tilde{f}_{\mathrm{up}}(r,z,t)=\tilde{f}_{\mathrm{low}}(r,-z,t)$ for all the cases investigated.

For the basic state, radial velocity and temperature are symmetric with respect to the midplane of the full zone, whereas the axial velocity is antisymmetric. For the disturbance modes, the same symmetry or the opposite case (all fields antisymmetric except for symmetric axial velocity) is possible in theory.[17] For the first case $G_{\mathrm{up}}=G_{\mathrm{low}}$, for the second, $G_{\mathrm{up}}=G_{\mathrm{low}}+\pi/m$. The present numerical results show that the azimuthal disturbances always exhibit antisymmetric behavior with respect to the equatorial plane, i.e., the latter case occurs (see, e.g., Fig. 7). According to these behaviors, Eq. (11) can be re-written as

$$F(r,z,\varphi,t)=F_o(r,z)+f(r,z,\varphi,t)$$
$$=F_o(r,z)+\tilde{F}_1(r,z,t)\sin(m\varphi+G_o), \qquad (12)$$

where G_o is a constant phase shift related to the azimuthal position of the disturbance with respect to $\varphi=0$ and $\tilde{F}_1(r,z,t)$ satisfies the conditions $\tilde{F}_1(r,z,t)=-\tilde{F}_1(r,-z,t)$ and $\tilde{F}_1(r,z=\pm 1,t)=0$. The behavior described above in terms of Eq. (12) is however only a simplified model, in fact, strong nonlinear interaction occurs between the toroidal convection rolls located in the upper part and lower part. In particular, Figs. 3, 7, 11, and 14 show that $f(r,z,\varphi,t)\neq 0$ for

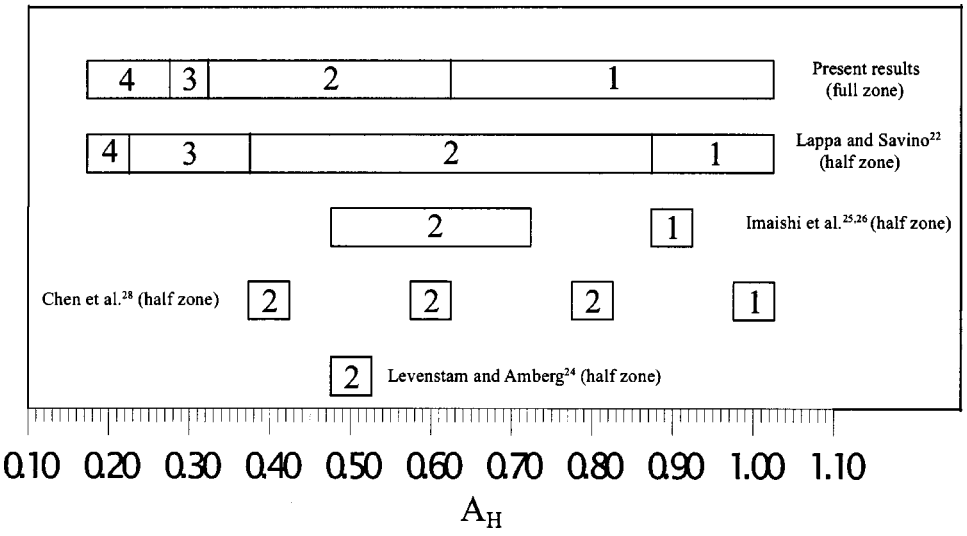

FIG. 17. Comparison between the azimuthal wave number of the full-zone configuration (present results) and available results dealing with the half zone configuration (Pr=0.01).

$z \to 0$. Since $\tilde{F}_1(r,z,t) \to 0$ for $z \to 0$, a second order function has to be present in the series expansion of $f(r,z,\varphi,t)$. The surface azimuthal velocity distribution can be expressed approximately as

$$V_\varphi(z,\varphi,t) = f(z,\varphi,t) \propto [\tilde{F}_1(z,t)\sin(m\varphi + G_o) - \tilde{F}_2(z,t)\sin(Nm\varphi + NG_o)], \quad (13)$$

where N is the "interaction factor" and $\tilde{F}_2(z,t)$ is a second-order contribute due to the interaction between the disturbances acting in the lower and upper halves: $\tilde{F}_2(z,t)$ satisfies the conditions $\tilde{F}_2(z,t) = \tilde{F}_2(-z,t)$ and $\tilde{F}_2(z,t) \to 0$ if $|z| > \xi$ with $0 < \xi < 1$, where ξ is the distance from the midplane at which the interaction between the upper and lower surface azimuthal flows can be considered negligible.

The numerical results shown in Fig. 3(a) for the case $A_F = 1.3$ and $m = 1$ are well fitted by Eq. (13) with $\tilde{F}_1(z) = z(1 - z^{2n_1})^2$ with $n_1 = 10$, $\tilde{F}_2(z) = A_2(1 - z^{2n_2})^2$ with $n_2 = 1$, $N = 4$ and $A_2 = 0.3$ [Fig. 3(b) shows the plot of the analytical expansion (13) with $\tilde{F}_1(z)$ and $\tilde{F}_2(z)$ given above, to be compared with Fig. 3(a)]. The value $N = 4$ leads to an "apparent" quadrupling of the azimuthal wave number of the azimuthal velocity distribution in the equatorial plane [i.e., the number of surface maxima of the azimuthal velocity in the midplane is quadrupled with respect to cross sections far from this plane; see, e.g., Figs. 6(a)–6(c)]. For $A_F < 1.3$, Eq. (13) and the previous expressions given for $\tilde{F}_1(z)$ and $\tilde{F}_2(z)$ still hold with $N = 2$ instead of $N = 4$ and $A_2 = 1$ [compare, e.g., Fig. 7(a) with Fig. 7(b) where the analytical expansion is plotted). This value leads to an "apparent" doubling of the azimuthal wave number of the azimuthal velocity distribution in the equatorial plane [see, e.g., Figs. 10(a), 10(b), 13(a), and 13(b)].

Note that, due to the antisymmetric behavior of the disturbances, the flow pattern at $z = 0.5$ appears to be rotated of π/m with respect to the flow pattern at $z = -0.5$ [Figs. 6(a)–6(c)].

In order to clarify why disturbances antisymmetric with respect to the equatorial plane are selected and amplified whereas z-symmetric disturbances never occur, some computations (in particular for $A_F = 0.5$, $A_F = 1.0$, $A_F = 1.5$) have been repeated under the constraint that the flow is symmetric with respect to the equatorial plane. Equations (2a)–(2c) have been solved for $0 \leqslant z \leqslant 1$ with the symmetry conditions ($0 \leqslant r \leqslant 1/A_F$; $0 \leqslant \varphi \leqslant 2\pi$)

$$V_z(z=0,r,\varphi,t) = 0, \quad (14a)$$

$$\frac{\partial V_r}{\partial z}(z=0,r,\varphi,t) = 0, \quad (14b)$$

$$\frac{\partial V_\varphi}{\partial z}(z=0,r,\varphi,t) = 0, \quad (14c)$$

$$\frac{\partial T}{\partial z}(z=0,r,\varphi,t) = 0. \quad (14d)$$

Figure 18 shows that the growth rate constants obtained in this case always lie below the corresponding ones obtained without any constraint for the flow. Hereafter the critical Marangoni number obtained under the constraint of disturbance symmetric with respect to the midplane will be referred to as $\mathrm{Ma}_c^{(s)}$. The computations show that for $A_F = 0.5$, $\mathrm{Ma}_{c1} = 9.76$, and $\mathrm{Ma}_{c1}^{(s)} = 18.255$, for $A_F = 1.0$, $\mathrm{Ma}_{c1} = 12.413$ and $\mathrm{Ma}_{c1}^{(s)} = 13.536$, for $A_F = 1.5$, $\mathrm{Ma}_{c1} = 10.154$, and $\mathrm{Ma}_{c1}^{(s)} = 13.53$. Therefore antisymmetric disturbances are selected and amplified since they are the most dangerous. Moreover for the case $A_F = 1.5$ the critical azimuthal wave number is $m = 1$ without constraints and $m = 2$ for the full zone z-symmetric case and for the half zone model showing (as expected) that the interaction between the upper and the lower rolls may play a critical role in the selection of the azimuthal wave number.

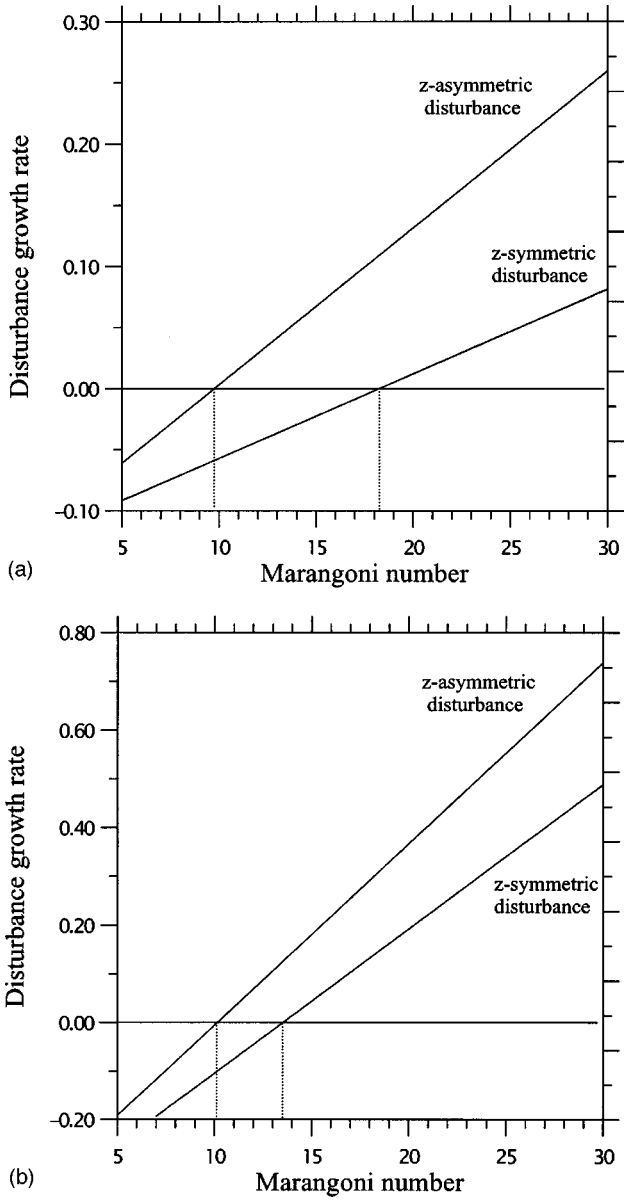

FIG. 18. Growth rates as function of the Marangoni number and determination of the first critical Marangoni number (mirror-symmetric and antisymmetric disturbances): (a) $A_F = 0.5$, (b) $A_F = 1.5$.

V. CONCLUSIONS

Instability of Marangoni convection in floating zones (full zone configuration) of a low Prandtl number fluid under

microgravity conditions has been investigated by direct three-dimensional and time-dependent solution of the Navier–Stokes equations. To overcome the prohibitive time required for the accurate simulation of the problem, a new parallel code has been developed and widely validated through a grid refinement study and comparison with results available in literature.

Due to the lack of numerical and experimental information and since, according to recent experimental results, this instability seems to play an important role in the crystallization process, the investigation has been focused in particular on the first (stationary) bifurcation to 3D flow. A parametric analysis (still absent in literature) of the influence of the aspect ratio of the liquid zone on the features of the three-dimensional instability of Marangoni flow has been carried out.

For the surface heat flux a novel distribution has been introduced corresponding to the radiative flux generated by a ring heater positioned around the equatorial plane of the full zone at a distance h from the free interface.

The critical wave number depends on the geometrical aspect ratio. It increases if the geometrical aspect ratio of the liquid column is decreased. While the critical wave number changes with the aspect ratio, the critical Marangoni number does not change much. For half zone configurations several investigators found Ma_c values which are two times higher than the values calculated for the present case of full zone. The reason for this difference is, that the independence and separation of the flows in the upper and the lower half of a full zone, which is stated by using a half zone model, is not true. The instability of the half zone flow is not relevant for the full zone configuration since the mirror symmetry with respect to the midplane is broken.

The present numerical results show in fact that the azimuthal disturbances always exhibit antisymmetric behavior with respect to the equatorial plane. Strong interaction occurs moreover between the toroidal convection rolls located in the upper part and lower part. This leads for some values of the aspect ratio to an ''apparent'' doubling or quadrupling of the azimuthal wave number of the azimuthal velocity distribution in the equatorial plane (i.e., the number of surface maxima of the azimuthal velocity in the midplane is doubled, or quadrupled with respect to cross sections far from this plane). The distribution of the azimuthal velocity disturbances on the free surface (never reported before) has been briefly discussed through a formal series expansion. Analytical expressions have been found for first and second order contributes in the series expansion and a new parameter (the interaction factor N) has been defined to characterize the complex surface flow pattern around the midplane and to explain the apparent doubling ($N=2$) or quadrupling ($N=4$) of the wave number that occurs there.

The occurrence of disturbances symmetric with respect to the equatorial plane has been investigated under the constraint of z-symmetric flow. The results have shown, as expected, that z-symmetric disturbances are not selected since they are characterized by larger values of the critical Marangoni number.

Further investigation is needed for the analysis of the influence of the volume of the liquid zone, the effect of the static and/or dynamic deformation of the liquid/gas interface and for the case of high Prandtl number liquids ($\mathrm{Pr}>1$).

ACKNOWLEDGMENTS

The author would like to thank Dr. H. C. Kuhlmann (University of Bremen) for some helpful discussions and the referees for the guidelines provided to the author and the constructive comments and suggestions.

[1] C. H. Chun, ''Experiments on steady and oscillatory temperature distribution in a floating zone due to the Marangoni convection,'' Acta Astronaut. **7**, 479 (1980).
[2] G. Chen and B. Roux, ''An analytical study of thermocapillary flow and surface deformations in floating zones,'' Microgravity Q. **1**(2), 73 (1991).
[3] A. Rybicki and J. M. Florian, ''Thermocapillary effects in liquid bridges. I. Thermocapillary convection,'' Phys. Fluids **30**, 1956 (1987).
[4] Y. Zhang and J. I. Alexander, ''Surface tension and buoyancy driven flow in a non-isothermal liquid bridge,'' Int. J. Numer. Methods Fluids **14**, 197 (1992).
[5] C. W. Lan and S. Kou, ''Thermocapillary flow and melt–solid interfaces in floating-zone crystal growth under microgravity,'' J. Cryst. Growth **102**, 609 (1990).
[6] J. C. Chen, C. F. Chu, and W. F. Ueng, ''Thermocapillary convection and melt–solid interface in the floating zone,'' Int. J. Heat Mass Transf. **37**, 1733 (1994).
[7] J. C. Chen and C. F. Chu, ''Numerical computation of fluid flow of floating-zone crystal growth of molybdenum,'' Int. J. Heat Mass Transf. **38**, 1841 (1995).
[8] J. C. Chen and H. K. Wu, ''Numerical computation of heat flow, fluid flow and interface shapes in the float zone of lithium niobate during a melting process,'' Int. J. Heat Mass Transf. **39**, 3707 (1996).
[9] E. Chenier, C. Delcarte, and G. Labrosse, ''Stability of the axisymmetric buoyant-capillary flows in a laterally heated liquid bridge,'' Phys. Fluids **11**, 527 (1999).
[10] G. Chen and B. Roux, ''Instability of thermocapillary convection in floating zones,'' Proceedings VIIIth European Symposium on Materials and Fluid Sciences in Microgravity, Brussels (Belgium), 12–16 April 1992, ESA SP-333, 73.
[11] J. C. Chen and G. H. Chin, ''Linear stability analysis of thermocapillary convection in the floating zone,'' J. Cryst. Growth **154**, 98 (1995).
[12] G. Kasperski, A. Batoul, and G. Labrosse, ''Up to the unsteadiness of axisymmetric thermocapillary flows in a laterally heated liquid bridge,'' Phys. Fluids **12**, 103 (2000).
[13] J. Baumgartl, M. Gewald, R. Rupp, J. Stierlen, and G. Muller, ''The use of magnetic fields and microgravity in melt growth of semiconductors: A comparative study,'' Proceedings VIIth European Symposium on Materials and Fluid Sciences in Microgravity, Oxford (United Kingdom), 10–15 September, ESA SP 295.
[14] A. Croll, Th. Kaiser, M. Schweizer, A. N. Danilewsky, S. Lauer, A. Tegetmeier, and K. W. Benz, ''Floating-zone and floating-solution-zone growth of GaSb under microgravity,'' J. Cryst. Growth **191**, 365 (1998).
[15] M. Levenstam, G. Amberg, T. Carlberg, and M. Andersson, ''Experimental and numerical studies of thermocapillary convection in a floating zone-like configuration,'' J. Cryst. Growth **158**, 224 (1996).
[16] C. W. Lan and C. H. Chian, ''Three-dimensional simulation of Marangoni flow and interfaces in floating-zone crystal growth,'' Third International Workshop on Modeling in Crystal Growth, 18–20 October 2000, Hauppauge, New York.
[17] M. Wanschura, H. C. Kuhlmann, and H. J. Rath, ''Instability of thermocapillary flow in symmetrically heated full liquid zones,'' Proceedings of the Journal of the Joint Xth European and VIth Russian Symposium on Physical Sciences in Microgravity, edited by V. S. Avduyevsky and V. I. Polezhaev, **1**, 172 (1997).
[18] D. Camel, P. Tison, and T. Carlberg, ''Floating zone crystal growth of Germanium,'' Proceedings of the Norderney Symposium on Scientific Results of the German Spacelab Mission D2, edited by P. R. Sahm, M. H. Keller, and B. Schiewe (1995), p. 494.
[19] M. Lappa and R. Savino, ''3D analysis of crystal–melt interface shape and Marangoni flow instability in solidifying liquid bridges,'' J. Comput. Phys. **180**, 751 (2002).

[20]R. K. Srivastava, P. A. Ramachandran, and M. P. Dudukovic, ''Interface shape in Czochralski grown crystals: Effect of conduction and radiation,'' J. Cryst. Growth **73**, 487 (1985).
[21]M. Lappa and R. Savino, ''Parallel solution of three-dimensional Marangoni flow in liquid bridges,'' Int. J. Numer. Methods Fluids **31**, 911 (1999).
[22]M. Lappa, R. Savino, and R. Monti, ''Three-dimensional numerical simulation of Marangoni instabilities in noncylindrical liquid bridges in microgravity,'' Int. J. Heat Mass Transf. **44**, 1983 (2001).
[23]J. Leypoldt, H. C. Kuhlmann, and H. J. Rath, ''Three-dimensional numerical simulations of thermocapillary flows in cylindrical liquid bridges,'' J. Fluid Mech. **414**, 285 (2000).
[24]M. Levenstam and G. Amberg, ''Hydrodynamical instabilities of thermocapillary flow in a half-zone,'' J. Fluid Mech. **297**, 357 (1995).
[25]N. Imaishi, S. Yasushiro, T. Sato, and S. Yoda, ''Three-dimensional numerical simulation of oscillatory Marangoni flow in a half zone of low Pr fluids,'' Material Research in low gravity II, Vol. 3792, pp. 344–352 (SPIE The International Society for Optical Engineering), 19–21 July 1999, Denver, Colorado.
[26]N. Imaishi, S. Yasushiro, T. Sato, and S. Yoda, ''Numerical simulation of three dimensional oscillatory flow in half zone bridges of low Pr fluid,'' Proceedings 292 of the 4th JSME-KSME Thermal Engineering Conference, 1–6 October 2000, Kobe, Japan, 272–282.
[27]S. Yasushiro, T. Sato, N. Imaishi, and S. Yoda, ''Three-dimensional Marangoni flow in liquid bridge of low Pr fluid,'' Space Forum **6**, 39 (2000).
[28]Q. S. Chen, W. R. Hu, and V. Prasad, ''Effect of liquid bridge volume on the instability in small-Prandtl-number half zones,'' J. Crystal Growth **203**, 261 (1999).